Available online at www.sciencedirect.com

ScienceDirect

Applied Catalysis B: Environmental 78 (2008) 80–91

APPLIED CATALYSIS B: ENVIRONMENTAL

www.elsevier.com/locate/apcatb

Non-aqueous sol–gel synthesis, characterization and catalytic properties of metal fluoride supported palladium nanoparticles

Pratap T. Patil [a], Anton Dimitrov [a], Holm Kirmse [b], Wolfgang Neumann [b], Erhard Kemnitz [a,*]

[a] Institute of Chemistry, Humboldt University Berlin, Brook-Taylor-Str. 2, 12489 Berlin, Germany
[b] Institute of Physics, Humboldt University Berlin, Newton-Str. 14, 12489 Berlin, Germany

Received 5 April 2007; received in revised form 23 June 2007; accepted 24 July 2007
Available online 27 July 2007

Abstract

High surface area (HS) metal fluoride supported palladium catalysts (Pd^0/MF_x) ($MF_x = AlF_3$, MgF_2, CaF_2 and $KMgF_3$) together with the respective Pd-free HS-MF_x catalysts have been prepared via a novel sol–gel synthesis. In a first step, the reaction of anhydrous hydrogen fluoride (aHF) with the respective solutions of the metal alkoxides containing up to 10% $Pd(acac)_2$ yielded the catalyst precursors as HS-gels. In a second step, gas phase fluorination followed by H_2-treatment was employed to obtain the final Pd^0/MF_x catalysts. X-ray diffraction (XRD) indicated the formation of mainly amorphous AlF_3 and Pd^0/AlF_3, whereas bulk MgF_2, CaF_2 and $KMgF_3$ and the respective Pd-loaded phases were partially crystalline. The XRD patterns of Pd^0/MF_x revealed besides the occurrence of broad MF_x-reflections only very weak reflections for Pd^0 supporting a uniform dispersion of Pd nanoparticles inside the highly distorted MF_x structures as it was independently reconfirmed by TEM-investigations. FTIR photo-acoustic spectroscopy with pyridine chemisorption (FTIR-PAS) and dismutation activities showed that AlF_3 and MgF_2 bulk as well as the supported Pd samples possess strong to moderate Lewis acidities. CaF_2 and $KMgF_3$ bulk as well as the respective Pd samples were found to be neutral. BET specific surface areas of MF_x and Pd^0/MF_x are very high, up to ten times higher than known from literature. TEM showed homogeneously dispersed Pd nanoparticles on MF_x matrices with a mean particle size of ~5 to 8 nm. Catalytic activities of the samples were tested for the conversion of $CHClF_2$ into valuable compounds by gas phase dismutation, hydrodehalogenation and pyrolysis, in presence as well as absence of hydrogen. Based on the obtained results and D/H-isotope exchange measurements, a carbene mechanism involving competitive dismutation coupled with consecutive reactions is proposed for the hydrodehalogenation process.

Keywords: Metal fluorides; Supported palladium nanoparticles; Sol–gel synthesis; $CHClF_2$ conversion; Hydrodehalogenation; CH_2F_2

1. Introduction

Difluoromethane (CH_2F_2, HFC-32) is an important compound used as low boiling refrigerant, substituting environmentally harmful former chlorine containing fluorocarbons. Fluorination of CH_2Cl_2 by SbF_5 [1] and/or by HF [2], as well as HF-fluorination of formaldehyde in presence of BF_3 [3] are well established methods for its synthesis on industrial scale. In addition, there are many reports focusing on the selective synthesis of hydrofluorocarbons by hydrodechlorination reaction of the respective chlorofluorocarbons, e.g. the formation of CH_2F_2 from dichlorodifluoromethane (CCl_2F_2, CFC-12) [4–8] or from chlorodifluoromethane ($CHClF_2$, HCFC-22) [9–16]. Because of the ''steady state availability'' of the latter compound – it is the key compound for manufacturing PTFE – a selective and efficient synthesis method for CH_2F_2 based on hydrodechlorination of $CHClF_2$ as starting material is of great practical interest. Thus, attempts have already been undertaken to selectively hydrodechlorinate $CHClF_2$ but conversion into the desired CH_2F_2 is very low, making a technical application senseless [10–13]. Palladium supported catalysts [17], more specifically on metal fluoride supports [18], have generally been applied for the hydrodechlorination of chlorine containing fluorocarbons. Due to their high thermal stability and resistance against HF and/or HCl, metal fluorides have been found to be advantageous over commonly used oxidic catalysts with respect to activity, stability and desired product selectivity [5,7,17]. For this purpose AlF_3 [4–6,10] and MgF_2 [9,10] are the most studied compounds to be used as supports.

* Corresponding author. Tel.: +49 30 2093 7555; fax: +49 30 2093 7277.
E-mail address: erhard.kemnitz@chemie.hu.berlin.de (E. Kemnitz).

0926-3373/$ – see front matter © 2007 Published by Elsevier B.V.
doi:10.1016/j.apcatb.2007.07.023

The structural and catalytic properties of the metal fluorides are strongly determined by the synthesis method and post synthesis treatments [19]. We have developed a novel two step non-aqueous sol–gel synthesis of nanoscopic, high surface area (HS) metal fluorides [20,21] producing materials with extra ordinary properties: AlF_3 prepared this way has not only a very large surface (up to 450 m^2/g) but also possess a nanoscopic, mesoporous and highly distorted structure. Its Lewis acidity is as high as that of SbF_5 and aluminium chlorofluoride (ACF), thus HS-AlF_3 is obviously – beside ACF [22] – the strongest solid Lewis acid known [23]. Our sol–gel method was successfully implemented for the synthesis of pure and modified fluorides, e.g. MgF_2 [24], $MgF_{2-x}(OH)_x$ [25], MgF_2 doped with FeF_3 [26] and CrF_3 [27], $AlF_{3-x}(OH)_x$ supported V_2O_5 [28], as well as for complex metal fluorides like $KAlF_4$ and $KMgF_3$ [29]. The basics of this new sol–gel synthesis route were reviewed recently summarizing the results within this method for preparing nano-structured metal fluorides [30]. A very important feature of this method is that it offers a possibility of implementing one or more components of interest into the HS metal fluorides, enabling high dispersion of "dopant" at nanoscopic scale.

As a part of exploring the synthesis of functionalized metal fluorides via this new route, we report here the preparation of metal fluorides supported palladium catalysts and their catalytic activities for the selective conversion of $CHClF_2$ to CH_2F_2. The aim was to explore to what extent tuning of Lewis acidity of the fluoride support together with the properties of the noble metals may have synergistic effects on the hydrodechlorination reaction. Therefore, we have chosen supports of varying Lewis acidity: AlF_3 (very strong), MgF_2 (moderate), CaF_2 and $KMgF_3$ (neutral). To understand bulk and surface properties of the catalyst, important intermediates as well as final catalysts have been characterized by different analytical techniques. Along with the target hydrodechlorination reaction, the catalytic activities have been studied for the dismutation reaction of $CHClF_2$ as well as for the pyrolysis and co-pyrolysis, which are competitive reactions depending on the reaction temperature.

2. Experimental

2.1. Chemicals

Palladium acetylacetonate (Fluka), aluminium isopropylate (Aldrich, 98%), magnesium (Aldrich, 99.98%), calcium (Aldrich, 99%), potassium *tert*-butoxide (Aldrich, 95%), $CHClF_2$ (FC-22) and other fluorocarbons used for analytical purpose of 99% purity (gifted by Solvay Fluor GmbH, Germany) were used as supplied. High purity (99.999%) gases (H_2 and N_2) were received from Air Berlin, D_2 (99.7%) from Messer Griesheim. Isopropanol and methanol were dried prior to use and stored over molecular sieves.

2.2. Catalysts synthesis

2.2.1. Synthesis of MF_x bulk supports

HS-AlF_3 [20] and HS-MgF_2 [24] were prepared as reported. For the synthesis of HS-CaF_2, Ca turnings were dissolved in a large excess of thoroughly dried methanol, and to the formed $Ca(OMe)_2$-solution a stoichiometric amount of methanolic solution of anhydrous hydrogenfluoride (aHF) was added under stirring and cooling. Although no sol formation was observed, a gel like product was obtained. After drying under vacuum at 50 °C the dry gel was post-fluorinated with gaseous $CHClF_2$. $KMgF_3$ was prepared similarly: here, methanolic aHF was added to a stoichiometric mixture of freshly prepared $Mg(OMe)_2$ and KO^tBu (Eq. (1)) followed by vacuum drying and gas phase post-fluorination by $CHClF_2$.

$$KO^tBu + Mg(OMe)_2 + 3HF \xrightarrow{MeOH} KMgF_3 + {}^tBuOH + 2MeOH \quad (1)$$

2.2.2. Synthesis of $Pd^{II}/MF_{x-y}(OR)_y$ catalyst precursors

Pd^{II}/AlF_3: 11.55 g of aluminium isopropylate was dissolved in a PTFE reactor in 100 ml ^{i}PrOH. 715 mg of $Pd(acac)_2$ dissolved in 2–3 ml chloroform was added to the vigorously stirred clear solution. Liquid phase fluorination by drop wise addition of HF/^{i}PrOH (HF/Al = ~3.1) led to the formation of yellowish colored sol, which was further stirred vigorously for 5 h and aged for 12–15 h. After drying at 65 °C under vacuum (4–5 h), the $Pd^{II}/MF_{x-y}(OR)_y$ precursor was obtained. MgF_2, CaF_2 and $KMgF_3$ supported Pd precursors were prepared similarly. [CAUTION: HF is a highly toxic and irritant compound causing severe burns if it comes in contact with skin. Appropriate safety precautions must be used].

2.2.3. Post fluorination of $Pd^{II}/MF_x(OR)_y$

All catalyst precursors were fluorinated with $CHClF_2$ in gas phase as follows: a sample of about 1.5 g was placed in the center of the reactor. $CHClF_2$ (flow rate 5 ml/min) and N_2 (20 ml/min) have been passed through, controlled by a digital mass flow meter (MKS instruments). The reactor temperature was controlled by a temperature regulator (HORST GmbH) and raised from 100 to 300 °C for 8–10 h.

2.2.4. Reduction of Pd^{II}/MF_x

The Pd^{II}/MF_x samples, post-fluorinated with $CHClF_2$, were reduced at 200 °C for 5 h by a mixture of hydrogen and argon (1:4; 75 ml/min) using a temperature programmed furnace and increasing the oven temperature by 3 °C/min. Pd^0/CaF_2 used for D_2 isotope exchange experiments was reduced by using D_2 instead of H_2. Pd^0/C for comparison purposes, prepared simply by impregnation, was similarly reduced.

2.3. Catalyst characterization

2.3.1. Elemental analysis

C, H, N-analysis was performed using Leco CHNS-932 analyzer with extension of VTF 900. Wherever necessary, analysis of chloride was carried out by mercurimetric titration after burning the substance in oxygen by the Schoeniger flask technique [31].

2.3.2. X-ray diffraction (XRD)

The phase composition and crystallinity of the samples were analyzed by X-ray powder diffraction which was carried out with XRD 7, Rich. Seiffert & Co., Freiberg using Cu Kα (Cu $K\alpha_{1,2}$, $\lambda = 1.5418$ A) radiation. The spectra were recorded at room temperature in the 2Θ-range of 5–70°.

2.3.3. Thermal analysis (TA-MS)

The thermal behavior was studied by TA-MS measurements. A NETZSCH thermoanalyzer STA 409 C *Skimmer*® system, equipped with a BALZERS QMG 421, was used to record the thermoanalytical curves (TG, DTA) [32]. A DTA-TG sample carrier system with platinum crucibles (baker, 0.8 ml) and Pt/PtRh10 thermocouples was used. A sample of 44–62 mg was measured versus empty reference crucible. Constant purge gas flow of 70 ml/min N_2/10% H_2 and heating rate of 10 K/min were applied. The determination of the initial (T_i), extrapolated onset (T_{on}^{ex}) and peak (T_P) temperatures was performed following international recommendations [33].

2.3.4. N_2 adsorption–desorption isotherm

Nitrogen adsorption measurements were carried out at −196 °C using Micromeritics ASAP 2020. The BET surface area, S_{BET}, was obtained by applying the BET equation [34]. The total pore volume was evaluated from the amount of nitrogen adsorbed at the highest relative pressure of 0.99. The pore-size distribution was estimated by applying the BJH method to the desorption isotherm [35]. Before each measurement, the samples were degassed at 4×10^{-3} mbar at 200 °C for 10–12 h.

2.3.5. FTIR photoacoustic spectroscopy (FTIR-PAS)

The Lewis acid sites (LPy) and Brønsted acid sites (BPy) were measured with FTIR photoacoustic spectroscopy after pyridine adsorption (FTIR-PAS). Pyridine was loaded at 150 °C, and the FTIR spectra of pyridine adsorbed samples were recorded with MTEC 200 photoacoustic cell (FTIR system 2000) Perkin-Elmer instrument at RT between 4000 and 400 cm^{-1}. The intensities of bands at 1445 cm^{-1} (LPy), 1490 cm^{-1} (LPy + BPy) and 1540 cm^{-1} (BPy) were used for the evaluation of LPy and BPy [36].

2.3.6. Temperature programmed desorption of ammonia (NH_3-TPD)

The strength of acidic sites was measured quantitatively by NH_3-TPD. Samples of about 200 mg were heated at 350 °C for 1 h under Ar, and thereafter ammonia was loaded at 120 °C. Then, the sample was purged in a nitrogen flow until no ammonia could be detected in the gas phase. After cooling down this sample to 80 °C, the desorption of NH_3 during heating (10 °C per minute) was monitored between 80 and 500 °C by FTIR (Perkin-Elmer System 2000). The total amount of NH_3 desorbed was determined by absorption in excessive sulfuric acid and back titration with NaOH.

2.3.7. Transmission electron microscopy (TEM)

Samples for TEM measurements were prepared by a two-step procedure. First the Pd^0/CaF_2 powder was dispersed in methanol applying ultrasonic bath. Second a single droplet of the methanol-Pd^0/CaF_2 dispersion was transferred to a TEM grid covered by a continuous carbon film. After complete evaporation of methanol the samples were studied in a TEM HITACHI H8110 operated at an acceleration voltage of 200 kV.

2.4. Catalytic reactions

The reactions under investigation were carried out in a fixed bed microflow reactor. Appropriate amounts of catalysts were placed at the center of a quartz reactor (l = 45 cm, i.d. = 4 mm) and flow rates of the gases were controlled by mass flow controllers. In a typical run of hydrodehalogenation, 0.25 ml volume of catalyst (∼180–280 mg Pd^0/MF_x) was used. Contact time (CT) was 1 s and the gas hourly space velocity (GHSV) 3600 h^{-1}, a $H_2/CHClF_2$ molar ratio of 7 was maintained by adjusting the flow rates: $CHClF_2$ (1.5 ml/min), H_2 (10.5 ml/min) and N_2 (3 ml/min). The reaction products were passed through 1 M NaOH and analyzed by offline gas chromatograph (GC, HP-5890) on PoraPLOT Q capillary column (30m × 0.32 mm i.d.). No efforts were made to quantify HCl and/or HF amounts in course of the reactions since it has been proven under analogous conditions in our lab [37] that the carbon mass balance was almost complete (100%) within the GC-detection limits. Hence, the amount of hydrogenated C1-compounds corresponds to the HX amount formed. To keep the analysis reasonably easy to handle, the amount of HX was, therefore, not followed. The identity of all products was additionally confirmed by ^{19}F and ^{1}H NMR.

2.4.1. D_2 isotope exchange measurements

The D/H-isotope exchange experiments were carried out in a quartz reactor with on-line coupled mass spectrometer. Initially Pd^0/CaF_2 (200 mg) was heated under vacuum at 350 °C for 2 h, and thereafter 5 mbar of a gas mixture from $CHClF_2$ and D_2 (1:7) was loaded thereafter. The changes of the gas phase composition during the reaction were analyzed by MS technique using a quadrapole mass spectrometer QMG4211 (Pfeiffer Vacuum GmbH). The detailed instrumental setup is described elsewhere [38].

3. Results and discussion

3.1. Synthesis

The well established sol–gel method for preparation of metal fluorides [30] has been modified in such a way, that the introduction of additional components like Pd into the colloidal system during the synthesis does not significantly influence the bulk and surface properties of the resulting gel: it is comparable to a gel from pure metal fluorides but it contains already the palladium precursor in a highly dispersed state. The post fluorination of the dry gel is necessary to exchange remaining –OR groups by –F in order to get a fully fluorinated, Lewis acidic catalyst [30]. The final H_2-treatment aimed the reduction of Pd^{II} and – as has been proven by XRD (Fig. 1) but especially by TEM measurements (Fig. 5) – resulted in the formation of the

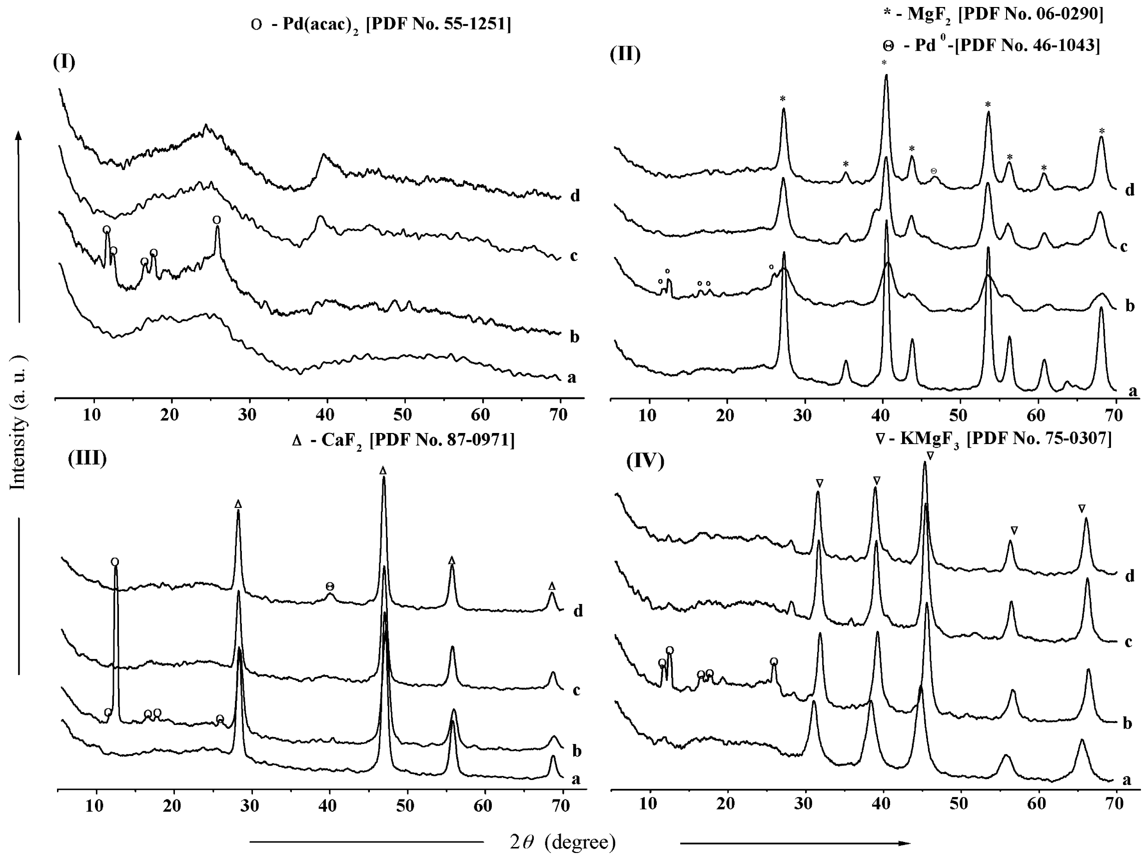

Fig. 1. XRD patterns of AlF_3 (I), MgF_2 (II), CaF_2 (III) and $KMgF_3$ (IV) based catalysts. (a) pure MF_x-supports, (b) $Pd^{II}/MF_{x-y}(OR)_y$-precursors, (c) Pd^{II}/MF_x-postfluorinated and (d) Pd^0/MF_x-reduced samples.

Pd-metal (no further indication for any PdF_2 or $PdCl_2$). It is of eminent importance to control the colloidal properties of the system (sol and gel formation, coagulation, peptisation, etc.) by optimizing the reaction conditions (temperature, stirring rate, type and amount of solvents) during the first fluorination step. At this stage, the –OR against –F exchange results in the formation of a viscous sol, which coagulates on further stirring to a three dimensional network of a polymeric semi-solid gel, the so called "wet gel". After ageing and vacuum drying a solid dry gel was obtained, denominated as catalyst "precursor" in this work. The elemental analysis of these precursors revealed significant amounts of carbon (17.7–27.3%) and hydrogen (4.8–6.1%) with varying values within the different metal fluoride supports (Table 1). The carbon content is mainly due to strongly adsorbed alcohol (solvent) as well as remaining unconverted alkoxide groups at the metal as has been already

Table 1
Elemental analysis, BET surface area and textural properties of bulk and palladium supported metal fluorides

Catalyst (cm^3/g)	Elemental analysis (%)[a]						$V_{BJH\text{-}d}$[b]	d_{avg} (Å)[c]	S_{BET} (m^2/g)[d]
	Pre.		Post-fluor.		AR				
	C	H	C	H	C	H			
AlF_3	23.9	5.9	0.8	0.2	–	–	0.47	84	225
MgF_2	2.3	1.6	<d.l.[e]	0.1	–	–	0.22	142	55.3
CaF_2	1.8	0.4	<d.l.	0.1	–	–	0.39	132	118
$KMgF_3$	2.1	1.1	<d.l.	0.0	–	–	0.52	139	148
Pd/AlF_3	25.6	5.5	1.8	0.3	1.6	0.4	0.33	125	106
Pd/MgF_2	3.7	1.9	1.4	0.1	1.4	0.4	0.16	83	78
Pd/CaF_2	4.9	1.5	1.3	0.2	1.2	0.2	0.27	185	59
$Pd/KMgF_3$	6.1	1.5	<d.l.	0.2	<d.l.	0.2	0.52	205	100

[a] Pre. = precursors, post-fluor. = post-fluorinated samples, AR = after reduction.
[b] BJH desorption cumulative pore volume of pores between 17.0 and 3000.0 Å diameters.
[c] Average pore diameter by BET.
[d] Specific surface area by BET.
[e] Below detection limit.

shown [20]. The surface areas and the Lewis acidic properties of the final catalysts depend on the synthesis parameters, like type of alkoxides and solvents, molar ratios, time of ageing and post fluorination conditions [39]. By using $CHClF_2$ as a post-fluorinating agent one can generate moderately acidic centers even on MgF_2 surface [24], a fluoride which had been prepared only as a neutral material up to now [40].

3.2. Characterization of catalysts

3.2.1. Elemental analysis, BET surface area and textural properties

The BET surface area, pore volume, pore diameter and elemental analysis data of the metal fluoride supported palladium catalysts together with the data of the corresponding ''sol–gel''-derived bulk metal fluorides are summarized in Table 1. The carbon and hydrogen contents of the precursors are quite high, indicating the presence of organics (adsorbed ROH and RO^-). Thus after the gas phase post-fluorination by $CHClF_2$, the organic is completely removed as evidenced by elemental analysis (Table 1). The pore diameters are between 83 and 205 Å typical for mesoporous materials. In case of supported Pd catalysts, the pore volumes are 28–56% smaller as those of the bulk metal fluoride materials. This decrease in pore volumes might be taken as a hint for the incorporation of Pd nanoparticles inside the pores of the metal fluoride matrices. This is in line with the observed decrease in surface areas on going from MF_x to Pd^0/MF_x (Table 1) as well as the homogeneous distribution of Pd on the support as evidenced by TEM images. The N_2 adsorption–desorption isotherms (not shown) are for all samples type IV adsorption isotherms with the characteristic H1 hysteresis: Such hysteresis is due to capillary condensation within the mesopores and is typical for mesopores with well ordered uniform shape and size [41]. On going from precursors to catalysts, we always observe significant losses in the BET specific surface areas. Nevertheless, the post-treated materials (Table 1) possess high surface areas which are up to ten times larger than reported from other preparations (AlF_3 [19,42], MgF_2 [40], CaF_2 [43], Pd^0/AlF_3 and Pd^0/MgF_2 [10]).

3.2.2. X-ray diffraction

In Fig. 1 the X-ray diffraction patterns of the products in course of the synthesis of metal fluorides supported Pd catalysts are shown. Additionally, the XRD of pure MF_X are included for comparisons. The characteristic diffractograms clearly depict the changes occurring on Pd during the steps of the catalyst preparation. Although the diffractograms of the precursor before and after gas phase fluorination have many features in common, there are some minor differences which need to be discussed. It is obvious that for some samples reflections at low 2 theta-values ($2\theta = 11.5$, $12.3°$) are present which disappear after gas phase fluorination and hydrogen treatment. These can clearly be ascribed to palladium acetylacetonate [PDF No. 55-1251] which was used as Pd^{II} precursor. It is obvious that they disappeared as a result of hydrogen treatment. Moreover, the weak reflection at $2\theta = 46.6°$ in case of the Pd^0/MgF_2 and at $2\theta = 40.1°$ in case of Pd^0/MgF_2 sample is indicative for the presence of Pd^0 [PDF No. 46-1043], however, obviously with a lower dispersion than in the other samples.

3.2.3. Thermal analysis coupled with mass spectrometry (TA-MS)

In order to get more insight into the reaction path during the Pd incorporation and understand the thermal behavior of the system, thermal analysis (TA) coupled with mass spectrometry (MS) investigations have been performed. Fig. 2 presents the TA-MS curves of a $Pd(II)/AlF_{3-x}(OiPr)_x$ catalyst precursor (25.6% C and 5.5% H) which shows the main processes during the catalyst formation. The TG curve exhibits a single step gradual weight loss of 23.7% up to 520 °C due to the loss of water and physically and chemically bonded organic moieties as confirmed by MS. The DTA curve shows exothermic peaks at 83, 134 and 545 °C which are caused by the reduction of Pd^{II} to Pd^0 by H_2, decomposition of –(OiPr) group and crystallization of aluminum fluoride, respectively. The decomposition of the remaining alkoxide at 134 °C is evidenced by the mass number 43 (C_3H_7) (Fig. 2) but the fact that it occurs exothermic is somehow unexpected. Probably the exothermic effect is due to H_2 gas used here which may result in the parallel formation of H_2O. The thermal behavior of the $Pd(II)/AlF_{3-x}(OiPr)_x$ system is very similar to that of $AlF_{3-x}(OiPr)_x$ except the observed lowering of crystallization temperature of HS-AlF_3 (546 against 563) [21] and the occurrence of acetyl (CH_3CO^+) fragment stemming from $Pd(acac)_2$ in the precursor matrix indicating the incorporation of acetylacetonate into the gel.

3.2.4. FTIR Photoaucoustic spectroscopy with pyridine adsorption

FTIR photoacoustic spectroscopy (FTIR-PAS) was employed for characterizing the acid sites of Pd^0/MF_x by using pyridine ($pK_a = 5.25$) as a basic probe molecule. Fig. 3 shows FTIR-PAS spectra of bulk (I, a–d) and metal fluoride supported Pd (II, a–d) samples. The vibration bands at 1451 (υ_{19b}), 1490 (υ_{19a}) and 1610 cm^{-1} (υ_{8a}) are characteristic for

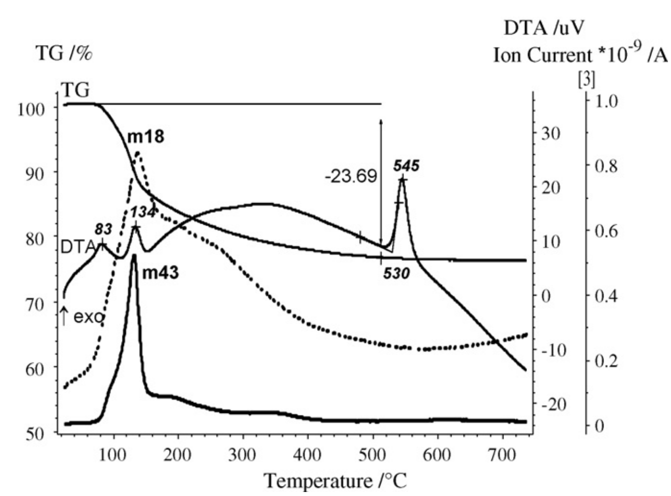

Fig. 2. TA-MS analysis of $Pd^{II}/AlF_{3-x}(OiPr)_x$ catalyst precursor with IC curves for m/z 18 for (H_2O^+) and m/z 43 (CH_3CO^+).

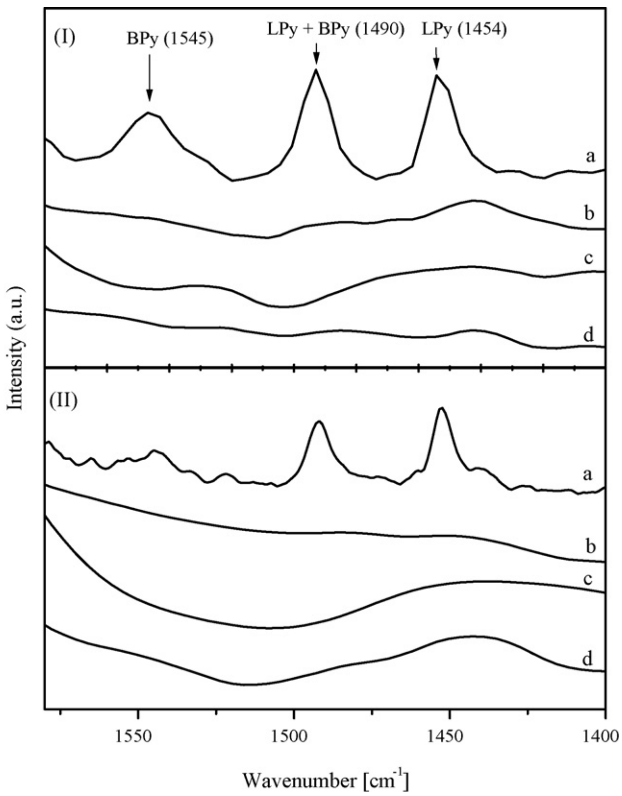

Fig. 3. FTIR photoacoustic spectra of pyridine chemisorption of (I) MF_x (a = AlF_3, b = MgF_2, c = CaF_2 and d = $KMgF_3$) and (II) Pd^0/MF_x (a = Pd^0/AlF_3, b = Pd^0/MgF_2, c = Pd^0/CaF_2 and d = $Pd^0/KMgF_3$) samples.

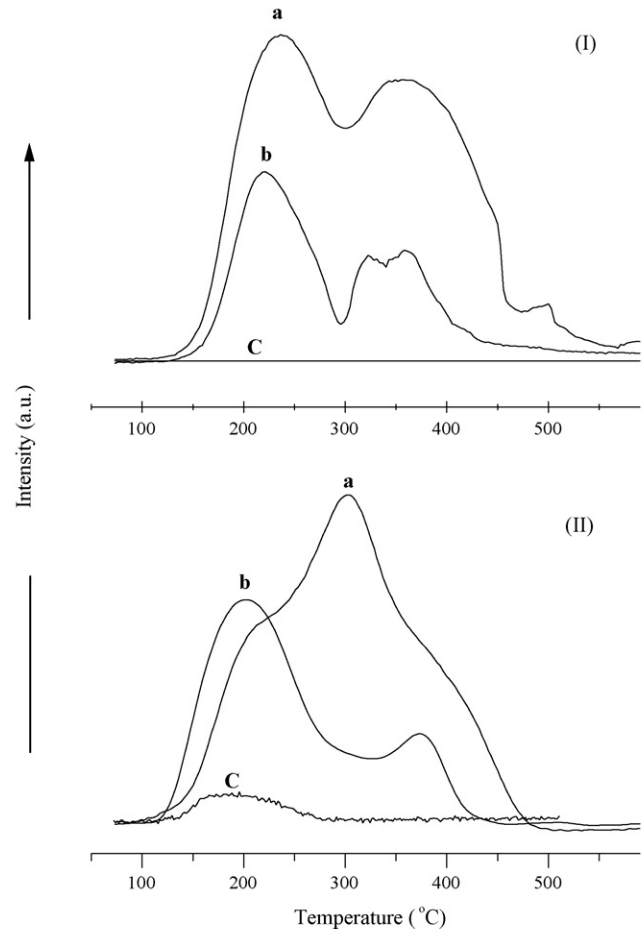

Fig. 4. NH_3-TPD profiles of (I) MF_x (a = AlF_3, b = MgF_2 and c = CaF_2) and Pd^0/MF_x (II) (a = Pd^0/AlF_3, b = Pd^0/MgF_2 and c = Pd^0/CaF_2) catalysts.

pyridine coordinated on Lewis acid sites (Lpy) and at 1490 (υ_{19b}), 1540 (υ_{19a}) and 1640 (υ_{8a}) on Brønsted acid centers (BPy) [36]. FTIR spectra confirm that the incorporation of Pd does not influence the acidic properties of MF_x supports. Especially in case of the AlF_3-system, both pure AlF_3 and Pd^0/AlF_3-samples contain Lewis acid sites. The peak around 1490 cm^{-1} is representative for Brønsted-sites only if it exceeds the intensity of the peak around 1450, but this is not the case here. No adsorption of pyridine was observed over MgF_2, CaF_2 and $KMgF_3$ based bulk as well as supported Pd samples, revealing the absence of acidic centers. However, both NH_3-TPD and catalytic dismutation indicated the presence of moderate acidic centers in MgF_2 and Pd^0/MgF_2 samples which obviously are too weak to be detected via pyridine FTIR. Moreover, it was shown that MgF_2 prepared via sol–gel synthesis clearly exhibits weak Lewis acid sites [24].

3.2.5. Temperature programmed desorption of ammonia (NH_3-TPD)

In Fig. 4, NH_3-TPD profiles of MF_x (I, a–c) and Pd^0/MF_x (II, a–c) samples are shown. Since the former FTIR-PAS results indicated exclusively Lewis sites and no Brønsted acid sites at all at the surface of the catalysts, these NH_3-TPD profiles give a clear picture of the strength distribution of these Lewis sites. The peak maxima at low temperatures (100–300 °C) correspond to weak acidic sites; the higher the desorption temperature is the stronger the sites are (300–425 °C – strong acid sites). Thus, the NH_3-TPD profiles characterize just the distribution of strength of acidic sites. The NH_3-desorption on AlF_3 and MgF_2 systems occurred at 475 and 400 °C, indicating the presence of strong and moderate acidic sites, respectively. Pure CaF_2 is not at all acidic, the weak desorption peak in case of Pd^0/CaF_2 around 200 °C is not significant and, hence, should not be taken as indicative for a considerable acid site since no catalytic dismutation activity was observed for this compound. The differences between MF_x and Pd^0/MF_x profiles are significant only in case of AlF_3. As a result of Pd loading, an additional acid site (intermediate strength) has obviously been formed. Since the FTIR-PAS does not give any hint to the formation of Brønsted sites, this is obviously a new medium strong Lewis site which could be generated on account of the strong sites in pure AlF_3 because the intensity of the deconvoluted peak (not shown) in the region 400–450 °C decreased as the intermediate strong site around 300 °C has increased. Obviously, incorporation of Pd into the sol-framework has altered the surface morphology on account of the strongest Lewis acid sites.

3.2.6. Microscopic study

The surface morphology, homogeneity and particle size was characterized by means of transmission electron microscopy (TEM), atomic force microscopy (AFM), and scanning electron microscopy (SEM).

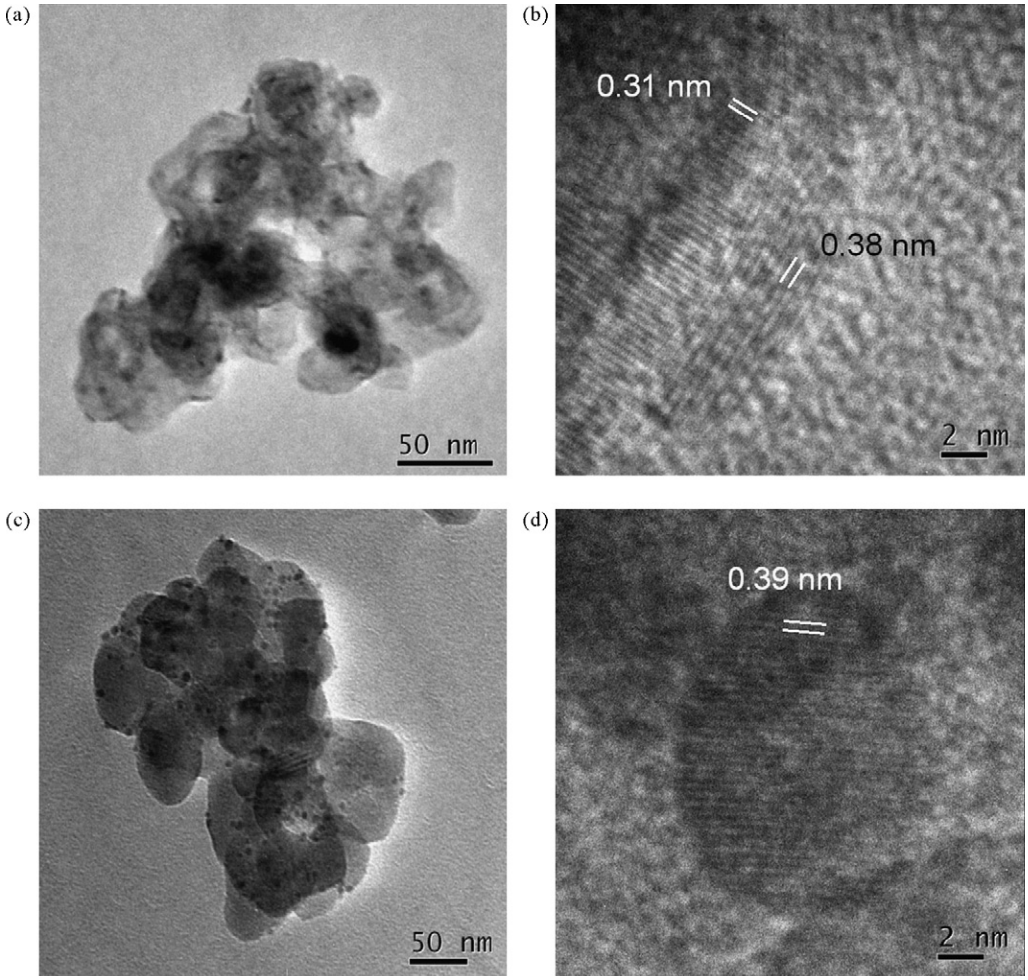

Fig. 5. TEM images of fresh (a, b) and used (c, d) Pd^0/CaF_2 catalysts used for hydrodehalogenation of $CHClF_2$.

TEM images of the Pd^0/CaF_2 system show exemplarily the dimension and distribution of the Pd-particles in the fluoride system (Fig. 5). Fig. 5a displays a characteristic bright-field image of a freshly prepared Pd^0/CaF_2 catalyst. The CaF_2 particles exhibit an irregular shape with diameters of about 40–50 nm whereas the Pd-particles can be recognized as darker spots with a diameter d ranging between 3 and 8 nm. Only a few bigger Pd-agglomerates (d ~15 nm) can be seen. Fig. 5b displays the border region of Pd^0/CaF_2 in high-resolution TEM mode. Basing on the distance of the marked lattice planes, two different phases can be distinguished. Within CaF_2 the distance of the {1 1 1} lattice planes of $d_{111} = 0.31(4)$ nm was determined and for metallic Pd the distance of the {1 0 0} lattice planes ($d_{100} = 0.38(2)$ nm). For all measured samples just these two phases were identified by TEM, meaning neither PdF_2 nor $PdCl_2$ is present. This clearly shows that Pd^{2+} has been quantitatively transformed into the metal stage as already predicted from XRD. A representative bright-field TEM image of a used Pd^0/CaF_2 catalyst is shown in Fig. 5c. As can be seen, the CaF_2 particle size has been increased ranging now from 50 to 80 nm. Moreover, the surface of the CaF_2 particles seems to be flattened as a result of the catalytic reactions which have taken place, thus being in line with the observed decrease of the BET surface area for the used catalysts (cf. Table 2). Interestingly enough, the Pd-particles appear more homogeneous in the used catalysts than in the fresh ones. The majority of Pd particles are spherical with a diameter in the range of 5–8 nm, whereas the larger dark areas observed in the fresh sample are minor and are mainly build of agglomerates of the smaller Pd-particles. The lattice plane distance of $d = 0.39(0)$ nm measured within the particle shown in the high-resolution TEM image of Fig. 5d for the used catalyst corresponds to the {1 0 0} lattice planes of Pd. However, since PdF_2 and PdO also exhibit lattice constants exactly with this value the formation of Pd^{II}-compounds due to the intensive contact with the highly corrosive gases HCl and HF cannot be excluded.

SEM investigations indicated for all the samples a homogeneous porous morphology, AFM images indicated a homogeneous dispersion of Pd nanoparticles (both not shown here) thus confirming the TEM results.

3.2.7. Used catalysts

The used catalysts were analyzed by XRD, elemental analysis and BET surface area measurements. A significant loss in surface area (50–70%) has been observed in case of AlF_3, MgF_2 and CaF_2 supported Pd catalysts used for hydrodehalogenation, but no coke formation and increase in

Table 2
Characterization of used catalysts

Reaction	Catalysts	Temp.[a] (° C)	Elemental analysis (%)		$V_{BJH\text{-}d}$[b] (cm^3/g)	d_{avg}[c] (Å)	S_{BET}[d] (m^2/g)
			C	Cl			
Hydrodehalogenation	Pd/AlF_3	350	2.2	0.4	0.36	484.9	30.9
	Pd/MgF_2	350	<d.l.	0.4	0.14	150.8	37.6
	Pd/CaF_2	400	0.8	1.1	0.15	256.5	24.6
	$Pd/KMgF_3$	400	1.0	3.4	0.52	238.9	90.0
Pyrolysis	AlF_3	600	19.6	2.3	0.03	166.6	9.2
	MgF_2	600	2.2	0.8	0.03	362.6	3.8
	CaF_2	600	20.0	2.4	0.07	166.6	18.1
Co-pyrolysis	CaF_2	700	36.7	1.7	0.04	174.7	10.6
	Pd/CaF_2	700	28.0	1.9	0.09	156.5	23.8

[a] Final reaction temperature.
[b] See footnotes of Table 1.
[c] See footnotes of Table 1.
[d] See footnotes of Table 1.

chlorine contents (Table 2). In case of $Pd^0/KMgF_3$ catalyst no significant loss in surface area and no any new phases in XRD (Fig. 6) were observed showing its stability. On contrary, AlF_3 based bulk and supported Pd catalyst underwent a transformation into crystalline α-AlF_3 (ASTM card no. 76-1623).

3.3. Conversion of $CHClF_2$ on MF_x based catalysts

The hydrodechlorination of $CHClF_2$ with the aimed formation of CH_2F_2 was the main objective of this work. However, it turned out that this is markedly affected by competitive dismutation and dehydrochlorination (elimination) reactions. Hence, these were carefully investigated, too.

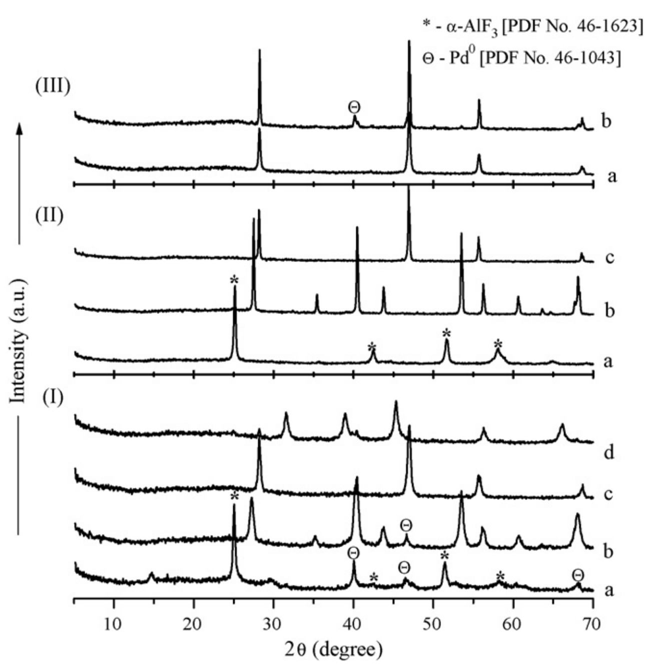

Fig. 6. XRD patterns of catalysts used for (I) hydrodehalogenation (a = Pd^0/AlF_3, b = Pd^0/MgF_2, c = Pd^0/CaF_2 and d = $Pd^0/KMgF_3$), (II) pyrolysis (a = AlF_3, b = MgF_2 and c = CaF_2) and (III) co-pyrolysis (a = CaF_2 and c = Pd^0/CaF_2) of $CHClF_2$.

3.3.1. Hydrodehalogenation versus dismutation

Hydrodehalogenation is one of the most used methods for the selective removal of halogens from halocarbons [44]. The kinetics (conversion and selectivity) of the halogen against hydrogen exchange on saturated halocarbons strongly depends on the strength of the C–X bonds, the nature of catalyst, and the reaction conditions. The formation of C–C-coupling products along with the desired CH_2F_2 have been reported for the reaction between $CHClF_2$ and hydrogen on Ni based catalysts [14], but CH_3F and CH_4 were the only products observed by when Pt on silica was used [15].

HS-AlF_3, one of the strongest solid Lewis acids known [20,21], was used as support expecting an enhancement of hydrodechlorination activity/selectivity by a synergistic effect between the strongly Lewis acidic support and the Pd-metal. However, in addition to the hydrodehalogenation products, CH_2F_2, CH_3F, and CH_4 (Eq. (2)), significant amounts of unexpected CHF_3 have been observed over Pd^0/AlF_3 (Table 1), showing a more complex reaction pathway. In case of hydrodehalogenation reactions over Pd, in a first step CH_2F_2 will be formed directly from $CHClF_2$. The other products, CH_3F and CH_4 may be formed by the consecutive hydrodefluorination of CH_2F_2 (Eq. (2)).

$$CHClF_2 \xrightarrow[-HCl]{H_2} CH_2F_2 \xrightarrow[-HF]{H_2} CH_3F \xrightarrow[-HF]{H_2} CH_4 \quad (2)$$

On the other hand, CHF_3 as a major reaction product contradicts clearly a hydrodehalogenation mechanistic path, but can easily be explained via two distinctly different reaction channels: (i) fluorination of the $CHClF_2$ by HF formed in the course of the above discussed consecutive hydrodefluorination, (ii) dismutation of $CHClF_2$ over the support according Eq. (3a). Since CHF_3 appears always immediately as the major compound (cf. Fig. 8, I), its formation via Cl/F-exchange according to path (i) must be excluded. Hence the only

plausible explanation is a reaction path proceeding via consecutive dismutation reactions of $CHClF_2$ on HS-AlF_3 according to Eqs. (3).

$$2\ CHClF_2 \longrightarrow CHCl_2F + CHF_3 \quad (3a)$$

$$2\ CHCl_2F \longrightarrow CHCl_3 + CHClF_2 \quad (3b)$$

$$5\ CHClF_2 \longrightarrow 3\ CHF_3 + CHCl_2F + CHCl_3 \quad (3)$$

Because the dismutation reactions on HS-AlF_3 surface could not be avoided, the observed high degree of conversion is doubtless caused by them according to Eqs. (3). The reactivity of the halocarbons increases with the number of chlorine atoms in the saturated haloalkane molecule, thus formation of hydrogenated compounds from chlorinated methane derivatives can easily be rationalized: $CHCl_2F \rightarrow CH_3F$; $CHCl_3 \rightarrow CH_4$. Since the starting compound, $CHClF_2$, dominantly undergoes dismutation reactions on the support, the formation of the desired CH_2F_2 on Pd is suppressed. CHF_3 is too stable to undergo hydrodefluorination reactions under these conditions; hence, the product distribution as listed in Table 3 can be fully understood this way. By considering dismutation reactions, the ratio of $CHCl_3$ to $CHCl_2F$ to CHF_3 must be constant irrespective of the conversion degree, even in case of the hydrodechlorinated products (CH_4, CH_3F, CHF_3). The observed yields are almost consistent with such interpretation. Moreover, a separate hydrodechlorination of $CHCl_3$ using Pd^0/AlF_3 yielded expectedly a complete conversion into methane.

The dismutation activity (conversion of $CHClF_2$) is very high over AlF_3, moderate over MgF_2 and negligible over CaF_2 in accordance to the Lewis acidic properties of the corresponding MF_x (Fig. 7). For instance, if once it has been activated at ~250 °C, the dismutation activity of *HS*-AlF_3 is as high as 98% even at 50 °C. The dismutation reactions even over moderate Lewis acidic MgF_2 [45] cannot be suppressed, and dominate the $CHClF_2$ conversion on Pd^0/MgF_2 (Table 3). In form of fine dispersed "nano-solids" as the result of our sol–gel method, CaF_2 and $KMgF_3$ were the only neutral compounds under investigation. In line with this, no dismutation was observed, but their activity concerning the hydrodechlorination reaction is, unfortunately, also low.

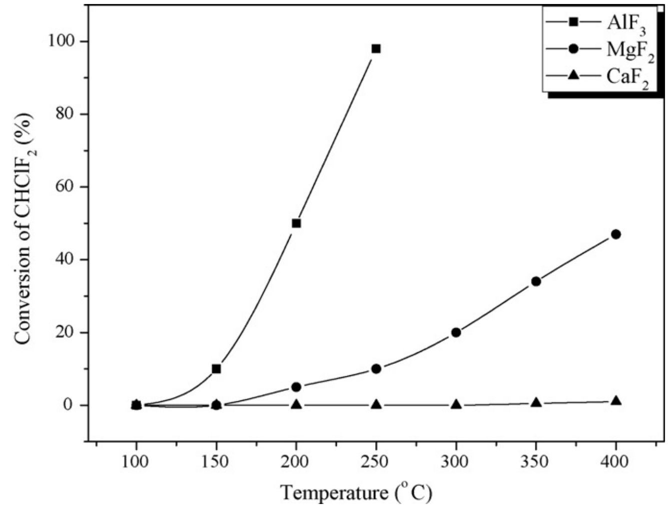

Fig. 7. Conversion of $CHClF_2$ in dismutation over bulk MF_x. Reaction conditions: amount of catalyst = 0.4 ml, CT = 1 s, GHSV = 3600 h^{-1}.

The results of the hydrodechlorination reactions using different kind of catalysts are summarized in Table 3. A Pd^0/C catalyst – widely used for hydrodehalogenation reactions – was employed for comparison reasons (Table 3). This catalyst too causes dismutation reactions like the Lewis acidic Pd^0/MF_x-catalysts to be seen by the formation of unwanted hydrogenated products. This behavior can be rationalized by the fact that activated carbon usually contains traces of metal salts from the synthesis procedure which can act as Lewis acid****. Analogous Pt-based catalysts were also prepared and tested. However, their catalytic performance was significantly lower, therefore, they will not be reflected here. In Fig. 8, the profiles of $CHClF_2$ conversion and product selectivity over Pd^0/AlF_3 and Pd^0/CaF_2 at various reaction temperatures are shown. A significant drop in $CHClF_2$ conversion over Pd^0/AlF_3 with gradual increase in temperature is accompanied by transformation of *HS*-AlF_3 into catalytically inactive α-AlF_3 as shown by XRD of used catalysts (Fig. 6). The phase transformation of HS-AlF_3 into crystalline α-AlF_3 does not occur at a defined temperature and differs depending on the degree of distortion [46], especially the phase transition temperature (290 °C) is unusually low and it was observed only in H_2 atmosphere. $CHClF_2$ conversion over Pd^0/CaF_2 at 320 °C was only 2.3% but

Table 3
Hydrodehalogenation of $CHClF_2$ with hydrogen over various metal fluorides supported palladium catalysts[a]

Sr. no.	Catalyst	Temp (°C)	$CHClF_2$ conv. (%)	Product selectivity (%)				
				CH_2F_2	CH_4	CHF_3	CH_3F	Other[b]
1.	Pd^0/AlF_3	260	85.9	0	32.1	31.5	28.2	8.2
2.	Pd^0/MgF_2	350	6.0	5.2	26.8	39.6	6.3	22.2
3.	Pd^0/CaF_2	350	2.3	72.7	27.3	0	0	0
4.	$Pd^0/KMgF_3$	350	2.9	68.6	31.4	0	0	0
5.	Pt^0/AlF_3	290	95.9	0	32.9	44.7	2.2	20.1
6.	Pt^0/MgF_2	290	0.6	0	48.7	51.3	0	0
7.	Pd^0/C	320	13.6	4.6	55.5	33.1	1.8	5.0

[a] Reaction conditions: amount of catalyst = 0.25 ml, $H_2/CHClF_2$ mole ratio = 7, GHSV = 3600 h^{-1}, CT = 1 s.
[b] CH_3Cl, CHF_2-CHF_2, C_2H_4, etc.

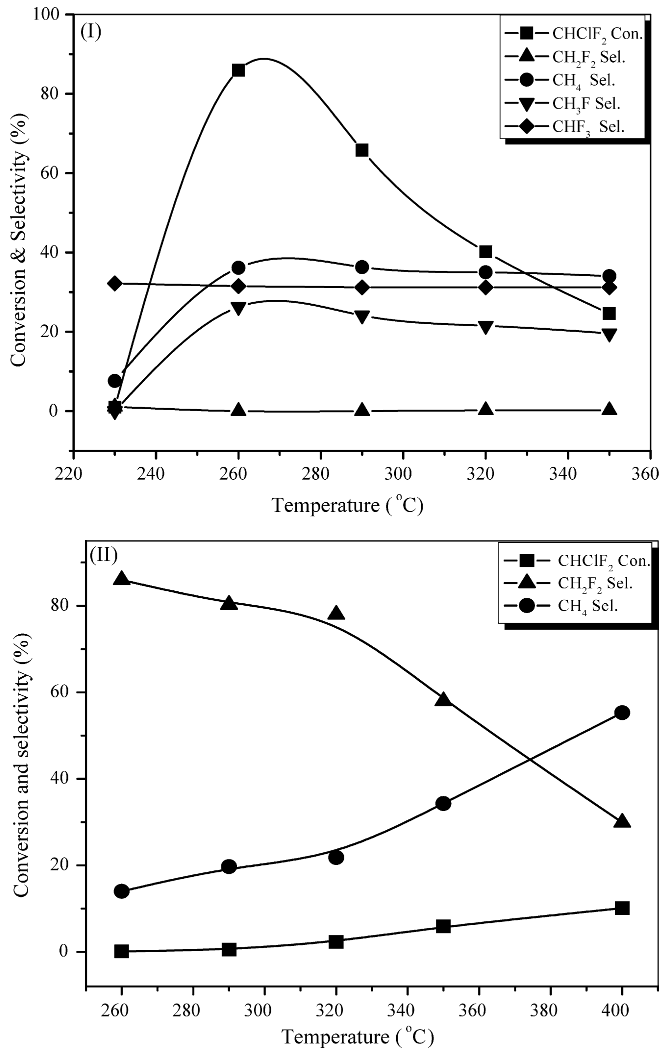

Fig. 8. Hydrodehalogenation of $CHClF_2$ over Pd^0/AlF_3 (I) and Pd^0/CaF_2 (II) catalysts. Reaction conditions: amount of catalyst = 0.25 ml, $H_2/CHClF_2$ mole ratio = 7, CT = 1 s, GHSV = 3600 h^{-1}.

CH_2F_2 and CH_4 were the only products observed with a selectivity of 78% and 22%, respectively (Fig. 8, II). The absence of side products, especially of CHF_3 can be taken as clear evidence that dismutation – expectedly – could successfully be suppressed. $CHClF_2$ conversion moderately increases by increasing the temperature (10% at 400 °C) but selectivity for CH_2F_2 (30%) and CH_4 (56 %) changes dramatically; some other products (~14%) are additionally formed. The formation of CH_2F_2 and CH_4 can be explained based on the carbene mechanism as explored for the hydrodechlorination of CCl_2F_2 and CF_3-CCl_2F, respectively [6,7,47]. The results of H/D isotope exchange measurements with $CHClF_2$ revealed the formation of HCl and DCl (Fig. 9), although H_2 was not present in the reaction system. Because HCl can only be generated from $CHClF_2$, its formation strongly supports the primarily formation of difluorcarbene as a result of HCl-elimination in analogy to the well known carbene mechanism [7], and so the formation of CH_2F_2 as a result of catalytic dehydrochlorination of $CHClF_2$ followed by hydrogenation of the formed difluorcarbene.

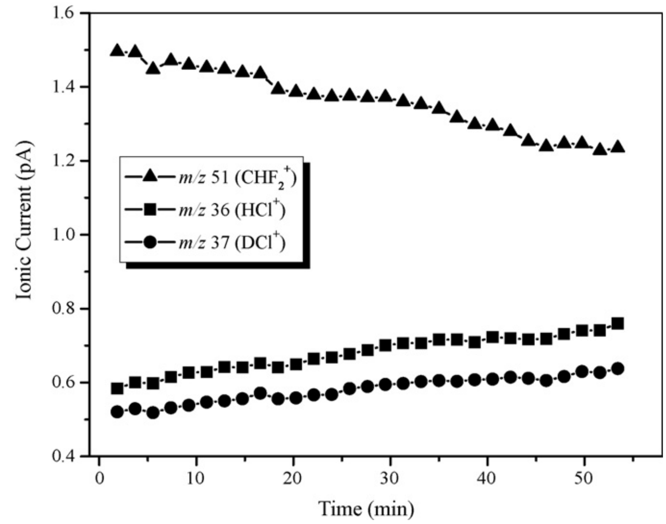

Fig. 9. IC curves for m/z 51 (CHF_2^+), m/z 35 (HCl^+) and m/z 36 (DCl^+) over Pd^0/CaF_2 catalyst.

3.3.2. Hydrodehalogenation versus dehydrochlorination

Summarizing the results obtained with the neutral metal fluoride supports, Pd^0/CaF_2 and $Pd^0/KMgF_3$, the following reaction pathway can be discussed (cf. also Scheme 1). In a first step, difluorcarbene is formed which becomes immediately hydrogenated by activated hydrogen on the Pd surface (Eq. (4a)). The absence of any CH_3F may be taken as a hint for the total suppression of dismutation reactions. Further on, it proves that even the hydrodefluorination must occur via an intermediately formed carbene. According to Eq. (4b), this time obviously a methylencarbene carbene is formed which further reacts with activated hydrogen to CH_4.

$$CHClF_2 \xrightarrow{-HCl} {}^{\bullet\bullet}CF_2 \xrightarrow{+2H} CH_2F_2 \tag{4a}$$

$$CH_2F_2 \xrightarrow{-2F} {}^{\bullet\bullet}CH_2 \xrightarrow{+2H} CH_4 \tag{4b}$$

The CF_2- and CH_2-carbenes are stable intermediates whereas a possible mixed carbine (fluorcarbene) is less probable, thus explaining the absences of CH_3F. However, at high temperatures, in presence of or even without any catalyst,

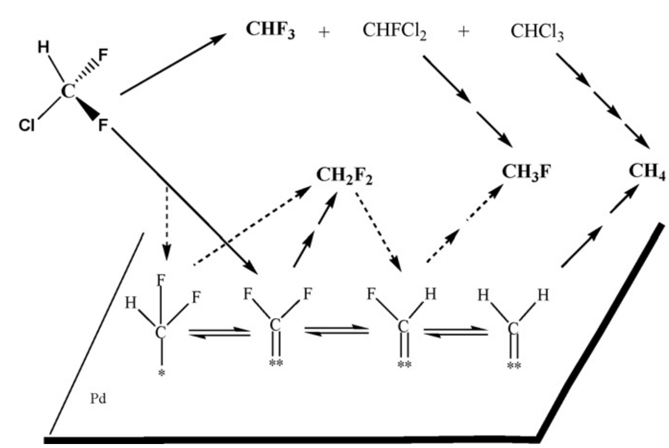

Scheme 1. Proposed reaction pathway for hydrodehalogenation of $CHClF_2$. Dismutation is the top cycle and the down cycle is hydrodechlorination.

dehydrochlorination followed by C–C coupling dominates the process (cf. Eq. (5)).

$$2CHClF_2 \xrightarrow{-2HCl} 2^{\bullet\bullet}CF_2 \rightarrow CF_2{=}CF_2 \quad (5)$$

3.3.3. Hydrodehalogenation versus C–C coupling dehydrochlorination (pyrolysis and co-pyrolysis)

Pyrolysis of $CHClF_2$ (Eq. (5)), which we consider further as C–C-coupling dehydrochlorination, is the well-known industrial process for manufacturing tetrafluoroethylene (TFE), the key intermediate for PTFE. It was long time considered that the TFE yield cannot be catalytically influenced. However, recently Sung et al. used AlF_3 and CaF_2 based catalysts and observed mild alterations by the metal fluorides [43]. To investigate if C–C-coupling and hydrogenation reactions can be controlled after the dehydrochlorination of $CHClF_2$ has occurred, we also performed pyrolysis and H_2-pyrolysis reactions over MF_x and Pd^0/MF_x catalysts. A non-catalytic run has also been carried out for comparison. Thus, we have tested our sol–gel prepared *high surface* metal fluorides for $CHClF_2$ pyrolysis at 600 °C aiming enhanced TFE selectivity. The catalytic activities in pyrolysis follow the order of $AlF_3 > MgF_2 >$ non-catalytic $> CaF_2$ with TFE selectivities following the order non-catalytic $> CaF_2 > MgF_2 > AlF_3$ at the initial period. However, with no any catalyst the TFE selectivity of the non-catalytic process was obtained (Fig. 10).

Since we were interested in CH_2F_2 formation, we intended to suppress the carbene dimerization according to Eq. (5) by adding hydrogen to the system. The dehydrochlorination of $CHClF_2$ in presence of hydrogen, co-pyrolysis, was investigated by Dolbier and coworkes [48] and yielded valuable

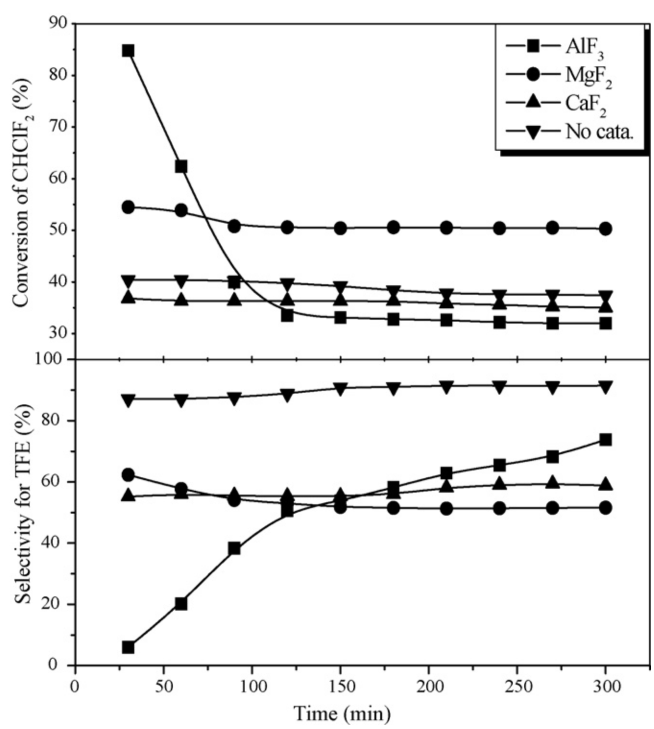

Fig. 10. Pyrolysis of $CHClF_2$ at 600 °C. Reaction conditions: amount of catalyst = 0.25 ml, CT = 1 s, GHSV = 3600 h^{-1}.

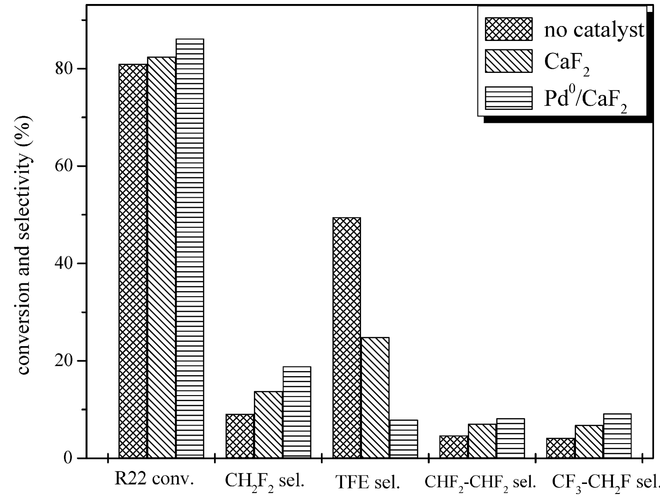

Fig. 11. Co-pyrolysis of $CHClF_2$ over CaF_2, Pd^0/CaF_2 and under non-catalytic conditions. Reaction conditions: amount of catalyst = 0.25 ml, $H_2/CHClF_2$ mole ratio = 5, temperature = 700 °C, CT = 1 s, GHSV = 3600 h^{-1}.

compounds like CHF_2–CHF_2 and CF_3–CH_2F, along with the formation of CH_2F_2 and $CF_2{=}CF_2$. In our experiments, expectedly higher amounts of CH_2F_2 were formed due to the addition of hydrogen, especially with the Pd^0/CaF_2 catalyst (Fig. 11), but still the TFE formation occurred to a noticeable degree. In presence of hydrogen, TFE was the major product observed by performing the non-catalytic reaction, but CH_2F_2 was the main product over Pd^0/CaF_2. Interestingly enough, in all cases the formation of CHF_2–CHF_2 and CF_3–CH_2F in noticeable amounts was observed. Most probably, these compounds were formed by a consecutive reaction of TFE with activated hydrogen.

4. Conclusions

The present work demonstrates an efficient non-aqueous soft chemical sol–gel method for the preparation of catalytically active high surface area metal fluoride supported palladium catalysts. Based on these results the following conclusions have been drawn:

- The non aqueous sol–gel synthesis for metal fluorides is a very effective tool to implement highly dispersed noble metals into the support. The metal fluoride supported catalysts exhibit a significantly higher surface area and mesoporosity as compared to classically prepared analogous ones. AlF_3 and Pd^0/AlF_3 samples are X-ray amorphous, and broad XRD reflections in MgF_2, CaF_2 and $KMgF_3$ based bulk as well as supported Pd samples reveal a high degree of distortion of the structures even for these materials.
- AlF_3 and Pd^0/AlF_3 samples are strongly Lewis acidic, MgF_2 and Pd^0/MgF_2 are moderately Lewis acidic and CaF_2 and $KMgF_3$ based bulk as well as supported Pd samples are neutral. Homogeneous dispersion of 5–8 nm Pd-particles in the fresh CaF_2-support (particle size ca. 30 nm) was detected by TEM. The used catalysts exhibited just minor changes in the Pd-particle size (ca. 5nm) but significant increase of the

support particle size (ca. 50 nm). The catalytic activity and product selectivity is strongly governed by the Lewis acidity of the supports. As expected, the strong Lewis acid supports activate very efficiently the C–Cl bond. However, it seems that also the C–F-bond becomes sufficiently enough activated to undergo halogen exchange reactions (dismutation) which is an undesired side reaction. By tuning down the Lewis acidity of the support to neutral surfaces these dismutation reactions can be totally suppressed. However, at the same time the C–Cl-bond activation goes down, too. This can be taken as a clear hint that not only the Pd-metal but to a great extend also the support has a remarkable influence on the C–X-bond activation. In order to overcome this problem, the reaction temperature has to be increased, this way opening the ‘‘window’’ to another unwanted side reaction – the C–C-coupling dehydrochlorination. Hence, at least three different reactions compete to each other, dismutation, hydrodechlorination and dehydrochlorination. Unfortunately, dismutation dominates in presence of Lewis acidic catalysts whereas neutral catalysts demand higher reaction temperatures at which dehydrochlorination reactions dominate. This way, there is no ‘‘reaction window’’ at which hydrodechlorination of $CHClF_2$ can be performed with high conversion degrees and high selectivities at the same time. However, for fluorine free chlorocarbons, the highly Lewis acidic nano-metal fluoride supported Pd catalysts seem to be superior because competitive dismutation cannot take place.

- Based of the catalytic results and H/D isotope exchange experiments a carbene mechanism involving dismutation coupled with consecutive hydrogenation reactions is proposed for hydrodehalogenation of $CHClF_2$ over metal fluorides supported Pd catalysts.
- As expected the catalysts used here are chemically robust even at elevated temperature (gas phase products are HCl and HF!), however the surface area declines significantly which is not only due to the high temperature but especially due to the presence of hydrogen and/or HX in the gas phase.

Acknowledgements

The authors thank Dr. M. Feist for TA-MS, Dr. K. Scheurell for H/D isotope exchange measurements and Mrs. S. Bäßler for TPD and FTIR measurements. This work was done with the support of EU in the FUNFLUOS Project, Contract No. NMP3-CT-2004-5005575.

References

[1] A.L. Henne, J. Am. Chem. Soc. 59 (1937) 1400.
[2] P. B. Logsdon, WO patent 24696 A1 (2000), to AlliedSignal Inc.
[3] J. L. Butcher, P.D. Bujac, WO patent 9506625 A1 (1995), to ICI.
[4] B. Coq, J.M. Cognion, F. Figueras, D. Tournigant, J. Catal. 141 (1993) 21.
[5] B. Coq, F. Figueras, S. Hub, D. Tournigant, J. Phys. Chem. 99 (1995) 11159.
[6] S. Deshmukh, J.L. d'Itri, Catal. Today 40 (1998) 377.
[7] E.J.A.X. van de Sant, A. Wiersma, M. Makkee, H. van Bekkum, J.A. Moulijn, Recl. Trav. Chim. Pays-Bas 115 (1996) 505.
[8] P.K. Ramarao, K.S. Ramarao, A.H. Padmasri, CATTECH 7 (2003) 218.
[9] A. Malinowski, W. Juszczyk, J. Pielaszek, M. Bonarowska, M. Wojciechowska, Z. Karpinski, J. Chem. Soc. Chem. Commun. (1999) 463.
[10] H. Berndt, H.H. Zahed, E. Kemnitz, M. Nickkho-Armiy, M. Pohl, J.M. Winfield, J. Mater. Chem. 12 (2002) 3499.
[11] A. Morato, F. Medina, J.E. Sueiras, Y. Cesteros, P. Salagre, L.C. De Menorval, D. Tichit, B. Coq, Appl. Catal., B 42 (2003) 251.
[12] A. Morato, C. Alonso, F. Medina, Y. Cesteros, P. Salagre, J.E. Sueiras, D. Tichit, B. Coq, Appl. Catal., B 32 (2001) 167.
[13] A. Morato, C. Alonso, F. Medina, J.L. Garreta, J.E. Sueiras, Y. Cesteros, P. Salagre, D. Tichit, B. Coq, Catal. Lett. 77 (2001) 141.
[14] A. Morato, C. Alonso, F. Medina, P. Salagre, J.E. Sueiras, R. Terrado, A. Giralt, Appl. Catal., B 23 (1999) 175.
[15] R. Hina, I. Arafa, A. Masadeh, React. Kinet. Catal. Lett. 87 (2006) 191.
[16] H. Yu, E.M. Kennedy, A.D. Azar, Y. Sakata, B.Z. Dlugogorski, Ind. Eng. Chem. Res. 44 (2005) 3442.
[17] F.J. Urbano, J.M. Marinas, J. Mol. Catal. 173 (2001) 329.
[18] B. Coq, F. Medina, D. Tichit, A. Morato, Catal. Today 88 (2004) 127.
[19] E. Kemnitz, D.H. Menz, Prog. Solid State Chem. 26 (1998) 97.
[20] E. Kemnitz, U. Groß, S. Rüdiger, C.S. Shekar, Angew. Chem. Int. Ed. 42 (2003) 4251.
[21] S.K. Rüdiger, U. Groß, M. Feist, H.A. Prescott, S.C. Shekar, S.I. Troyanov, E. Kemnitz, J. Mater. Chem. 15 (2005) 588.
[22] T. Krahl, R. Stösser, E. Kemnitz, G. Scholz, M. Feist, G. Silly, J.-Y. Buzare, Inorg. Chem. 42 (2003) 6474.
[23] J. Krishna Murthy, U. Gross, S. Rüdiger, V.V. Rao, V.V. Kumar, A. Wander, C.L. Baily, N.M. Harrison, E. Kemnitz, J. Phys. Chem. B 111 (2006) 8314.
[24] J. Krishna Murthy, U. Gross, S. Rüdiger, E. Kemnitz, J.M. Winfield, J. Solid State Chem. 179 (2006) 743.
[25] H.A. Prescott, Z.-J. Li, E. Kemnitz, J. Deutsch, H. Lieske, J. Mater. Chem. 15 (2005) 4616.
[26] J.K. Murthy, U. Groß, S. Rüdiger, E. Kemnitz, Appl. Catal., A 278 (2004) 133.
[27] J.K. Murthy, U. Groß, S. Rüdiger, E. Ünveren, W. Unger, E. Kemnitz, Appl. Catal., A 282 (2005) 85.
[28] K. Scheurell, E. Kemnitz, J. Mater. Chem. 15 (2005) 4845.
[29] M. Ahrens, G. Scholz, M. Feist, E. Kemnitz, Solid State Sci. 8 (2006) 798.
[30] S. Rüdiger, U. Groß, E. Kemnitz, J. Fluorine Chem. 128 (2007) 353.
[31] Schöniger, Mikrochim. Acta (1956) 869.
[32] E. Kaisersberger, E. Post, Thermochim. Acta 295 (1997) 73.
[33] J.O. Hill (Ed.), For Better Thermal Analysis III, Special Edition of the International Confederation for Thermal Analysis (ICTA), 1991.
[34] S. Brunauer, P.H. Emmett, E.J. Teller, J. Am. Chem. Soc. 60 (1938) 309.
[35] E.P. Barret, L.G. Joyner, P.P. Halenda, J. Am. Chem. Soc. 73 (1953) 373.
[36] A. Hess, E. Kemnitz, J. Catal. 149 (1994) 449.
[37] A. Hess, E. Kemnitz, Appl. Catal., A 82 (1992) 247.
[38] I.K. Murwani, E. Kemnitz, T. Skapin, M. Nickkho-Amiry, J.M. Winfield, Catal. Today 88 (2004) 153.
[39] S. Rüdiger, G. Eltnany, U. Groß, E. Kemnitz, J. Sol–Gel Sci. Technol. 41 (2007) 749.
[40] E. Kemnitz, Y. Zhu, B. Adamczyk, J. Fluorine Chem. 114 (2002) 163.
[41] G. Leofanti, M. Padovan, G. Tozzola, Catal. Today 41 (1998) 207.
[42] W. Kleist, C. Haeßner, O. Storcheva, K. Köhler, Inorg. Chim. Acta. 359 (2006) 4851.
[43] D.J. Sung, D.J. Moon, S. Moon, J. Kim, S.-I. Hong, Appl. Catal., A 292 (2005) 130.
[44] F. Alonso, I.P. Beletskaya, M. Yus, Chem. Rev. 102 (2002) 4009.
[45] M. Wojciechowska, M. Zielinski, M. Pietrowski, J. Fluorine Chem. 120 (2003) 1.
[46] U. Gross, S. Rüdiger, E. Kemnitz, K.-W. Brzezinka, S. Mukhopadhyay, C. Bailey, A. Wander, N. Harrison, J. Phys. Chem. A (2007), doi:10.1021/jp072388r.
[47] V.Y. Borovkov, F. Lonyi, V.I. Kovalchuk, J.L. d'tri, J. Phys. Chem. B 104 (2000) 5603.
[48] R. Romelar, V. Kruger, J. Marshall, W.R. Dolbier Jr., J. Am. Chem. Soc. 123 (2001) 6767.